Out-of-Band Effects of Satellite Ocean Color Sensors

Menghua Wang[1,*], Puneeta Naik[1,2], and SeungHyun Son[1,2]

[1]NOAA/NESDIS Center for Satellite Applications and Research
E/RA3, 5830 University Research Court
College Park, MD 20740, USA

[2]CIRA, Colorado State University, Fort Collins, CO 80523, USA

*Corresponding author: Menghua.Wang@noaa.gov

Applied Optics

Revised on 1/30/16

ABSTRACT

We analyze the sensor out-of-band (OOB) effects for satellite ocean color sensors of the Sea-viewing Wild Field-of-view Sensor (SeaWiFS), the Moderate Resolution Imaging Spectroradiometer (MODIS), and the Visible Infrared Imaging Radiometer Suite (VIIRS) for phytoplankton-dominated open oceans and turbid coastal and inland waters, following the approach of *Wang et al.* (2001) [Appl. Opt. 40, 342–348 (2001)]. The applicability of the open ocean water reflectance model of the *Morel and Maritorena* (2001) (MM01) [J. Geophys. Res. **106**, 7163–7180 (2001)] for the sensor OOB effects is analyzed for oligotrophic waters in Hawaii. The MM01 model predicted OOB contributions for oligotrophic waters are consistent with the result from in situ measurements. The OOB effects cause an apparent shift in sensor band center wavelengths in radiometric response, which depends on both the sensor spectral response function and the target radiance being measured. Effective band center wavelength is introduced and calculated for three satellite sensors and for various water types. Using the effective band center wavelengths, satellite and in situ measured water optical property data can be compared more meaningfully and accurately. It is found that for oligotrophic waters the OOB effect is significant for SeaWiFS 555 nm band (and somewhat 510 nm band), MODIS 412 nm

band, and VIIRS 551 nm band. VIIRS and SeaWiFS have similar sensor OOB performance. For coastal and inland waters, however, the OOB effect is generally not significant for the all three sensors, even though some small OOB effects do exist. This study highlights the importance of understanding the sensor OOB effect and the necessity of a complete prelaunch sensor characterization on the quality of ocean color products. Furthermore, it shows that hyperspectral in situ optics measurements are preferred for the purpose of accurately validating satellite-measured normalized water-leaving radiance spectra data.

OCIS codes: (010.0010) Atmospheric and oceanic optics; (010.1285) Atmospheric correction; (010.0280) Remote sensing and sensors; (010.4450) Oceanic optics.

1. INTRODUCTION

Since the success of the Coastal Zone Color Scanner (CZCS) mission [1, 2], several ocean color satellite sensors capable of routine global coverage have been launched, e.g., the Sea-viewing Wild Field-of-view Sensor (SeaWiFS) [3], the Moderate Resolution Imaging Spectroradiometer (MODIS) on the Terra and Aqua satellites [4], the Medium-Resolution Imaging Spectrometer (MERIS) on the Envisat [5], and the Visible Infrared Imaging Radiometer Suite (VIIRS) on the Suomi National Polar-orbiting Partnership (SNPP) [6, 7]. Table 1 provides the specifications of ocean color spectral bands for SeaWiFS, MODIS, and VIIRS, which may be different from the actual nominal center wavelengths. The nominal center wavelength is defined as the center wavelength measured from the band full-width at half-maximum (FWHM) of the sensor spectral response function (SRF). Satellite ocean color data products such as chlorophyll-a (Chl-a) concentration [8] and water diffuse attenuation coefficient at the wavelength of 490 nm $K_d(490)$ [9-11] have been extensively used to study global and regional oceanic phenomena [12-17]. For satellite ocean color remote sensing, a complete pre-launch characterization of sensor performance is essential in order to obtain accurate sensor-measured top-of-atmosphere (TOA) radiances that are then used to produce high quality ocean color products [18, 19]. Most satellite ocean color sensors have broad spectral bands; hence they not only have an in-band response, but also an out-of-band (OOB) response [20, 21]. The in-band response can be referred to integrated response within 1% relative to the peak response of the sensor spectral band, while the total-band response is the integrated response over the entire response of the sensor spectral band. Alternatively, following *Wang et al.* (2001) [21], for ocean color remote sensing we can approximate the in-band response as the sensor response at the band nominal center wavelengths. The OOB contribution can be defined as radiance difference in spectral response between the total-band and that of in-band (or relative difference between the two). In effect, the OOB contribution introduces a radiometric bias (relative to the sensor nominal center wavelength) with a magnitude in the range of about several percent and may have an adverse effect on the quality of ocean color products [21]. It should be noted that in the satellite ocean color data processing (particularly atmospheric correction) [18, 22, 23], all radiance components (e.g., atmospheric contributions) in the ocean-atmosphere system are computed (or approximated) using sensor SRF weighted calculations [20, 21]. *Gordon* (1995) [20] and *Wang et al.* (2001) [21] provided detailed descriptions and discussions about this process. Thus, the sensor SRF weighted normalized water-leaving radiance spectra $nL_w(\lambda)$ are derived from atmospheric correction [21]. Our discussion in this study focuses on the OOB effect on the satellite-derived $nL_w(\lambda)$ spectra, which are the key data for deriving all ocean biological and biogeochemical products, e.g., Chl-a concentration, ocean inherent optical properties (IOPs), water diffuse attenuation coefficients $K_d(490)$, etc. [8, 10, 11, 24-26].

A significant sensor OOB response can cause an increase or decrease in the observed radiance above the measurement at the nominal center wavelength [21, 27]. It is particularly noted that the OOB contribution for ocean color remote sensing is determined not only by the sensor OOB response, but also importantly by the target radiance that is measured [21]. Hence, different water types exhibit various degrees of the OOB contributions [21]. In addition, a significant sensor OOB response effectively causes a spectral shift in the band center wavelength from the nominal center wavelength, i.e., the spectral/optical effective band center wavelength is different from the nominal center wavelength. Although a correction (or conversion) for the OOB effect can be applied to the satellite ocean color data processing [21] based on the open ocean reflectance models [28, 29], relatively less is known about the satellite sensor OOB effect for the in situ measured radiances from both oligotrophic waters and particularly turbid coastal/inland waters. In addition, VIIRS OOB effects in ocean color remote sensing have not been investigated. It is noted that for the NASA satellite ocean color data processing the OOB correction based on the *Wang et al.* (2001) algorithm [21] with the *Morel and Maritorena* (2001) (MM01) [29] reflectance model has been used [30]. Furthermore, the NASA OOB correction has used the bandwidth of 10 nm for sensor spectral bands instead of the nominal center wavelength. In this study, we analyze the sensor OOB effect and determine the spectral effective band center wavelengths for the three satellite ocean color sensors (particularly focusing on VIIRS) with three cases: (1) modeled normalized water-leaving reflectance spectra using the *Morel and Maritorena* (2001) model [29] (MM01) for Chl-a concentrations ranging from 0.01 to 10.0 mg m^{-3}, (2) oligotrophic oceanic waters—in situ data from Marine Optical Buoy (MOBY) in Hawaii [31], and (3) productive and turbid waters—examples of the in situ data from the Chesapeake Bay (CB), East China Sea (ECS), and inland Lake Taihu [17, 32-34].

2. DATA AND METHODS

The in situ water optics data used in this study were obtained from various resources. In situ hyperspectral normalized water-leaving radiance ($nL_w(\lambda)$) (the definition of $nL_w(\lambda)$ refers to references [18, 35-37]) data from MOBY in the waters off Hawaii [31] were obtained from the NOAA CoastWatch website (http://coastwatch.noaa.gov/moby/). The Chesapeake Bay in situ optics data were obtained from the NASA SeaWiFS Bio-optical Archive and Storage System (SeaBASS) (http://seabass.gsfc.nasa.gov/) [32], representative of productive but moderately turbid waters [16, 38]. The East China Sea and inland Lake Taihu in situ $nL_w(\lambda)$ spectra were from previous studies [17, 33, 34], which provide data typical of highly turbid coastal and inland waters. In addition, the open ocean Case-1 water reflectance model MM01 [29] was used to simulate hyperspectral $nL_w(\lambda)$ data for various Chl-a concentrations from 0.01 to 10.0 mg m^{-3}. Figure 1 shows examples of the in situ normalized water-leaving reflectance $\rho_{wN}(\lambda)$ as a function of the wavelength for waters over Hawaii MOBY site, the Chesapeake Bay, East China Sea, and China's inland Lake Taihu. Note that $\rho_{wN}(\lambda) = \pi\ nL_w(\lambda)/F_0(\lambda)$ [18, 22], where $F_0(\lambda)$ is the extraterrestrial solar irradiance [39]. It is quite obvious from results in Fig. 1 that $\rho_{wN}(\lambda)$ spectra are significantly different from these four regions, in particular, Case-1 waters in Hawaii MOBY site have a significant different spectral distribution in $\rho_{wN}(\lambda)$ compared with those from coastal and inland waters.

For ocean color remote sensing, satellite-measured total-band and in-band normalized water-leaving radiances $nL_w(\lambda)$ can be calculated using the following formulae [21]:

$$nL_w^{(Total)}(\lambda_i) = \frac{\int_{\text{All}} nL_w(\lambda)\, S_i(\lambda)\, d\lambda}{\int_{\text{All}} S_i(\lambda)\, d\lambda} \tag{1}$$

and

$$nL_w^{(In\text{-}Band)}(\lambda_i) = \frac{\int_{S_i\left(\lambda^{(\pm)}\right)=1\%} nL_w(\lambda)\, S_i(\lambda)\, d\lambda}{\int_{S_i\left(\lambda^{(\pm)}\right)=1\%} S_i(\lambda)\, d\lambda}, \tag{2}$$

where $S_i(\lambda)$ is the corresponding sensor SRF for band i. It is noted that the in-band integration in Eq. (2) is from $\lambda^{(-)}$ corresponding to $S_i(\lambda^{(-)}) = 1\%$ to $\lambda^{(+)}$ corresponding to $S_i(\lambda^{(+)}) = 1\%$, relative to the $S_i(\lambda)$ peak value. The $S_i(\lambda)$ for SeaWiFS, MODIS, and VIIRS wavebands are provided in Fig. 2, showing sensor in-band and out-of-band responses. Note that these $S_i(\lambda)$ data are pre-launch sensor SRF measurements.

Satellite sensor-measured total-band and in-band signals can also be defined in the reflectance unit. With the definition of the sensor-measured normalized water-leaving reflectance $\rho_{wN}(\lambda)$ [18, 22], Eqs. (1) and (2) become:

$$\rho_{wN}^{(Total)}(\lambda_i) = \frac{\int_{\text{All}} \rho_{wN}(\lambda)\, F_0(\lambda)\, S_i(\lambda)\, d\lambda}{\int_{\text{All}} F_0(\lambda) S_i(\lambda)\, d\lambda} \tag{3}$$

and

$$\rho_{wN}^{(In\text{-}Band)}(\lambda_i) = \frac{\int_{S_i\left(\lambda^{(\pm)}\right)=1\%} \rho_{wN}(\lambda)\, F_0(\lambda)\, S_i(\lambda)\, d\lambda}{\int_{S_i\left(\lambda^{(\pm)}\right)=1\%} F_0(\lambda)\, S_i(\lambda)\, d\lambda}. \tag{4}$$

It is particularly noted that sensor-measured normalized water-leaving reflectance $\rho_{wN}(\lambda)$ spectra (or similarly remote sensing reflectance, defined as $R_{rs}(\lambda) = \rho_{wN}(\lambda)/\pi$) are weighted by $F_0(\lambda)S_i(\lambda)$ in the integration as shown in Eqs. (3) and (4). In this study, the spectral resolution of the in situ data is generally ~1 nm, and all data ($\rho_{wN}(\lambda)$, $F_0(\lambda)$, and $S_i(\lambda)$) were interpolated to the same 0.1 nm for carrying out the integrations in Eqs. (1)–(4). The numerical integrations are quite accurate, much more accurate than those from in situ measurements, the model $\rho_{wN}(\lambda)$ data, or solar irradiance $F_0(\lambda)$ data. Thus, uncertainties in the calculations (integrations) are mostly from the integrand data, and not from the numerical integrations.

The sensor OOB contribution in $\rho_{wN}(\lambda)$ (or $nL_w(\lambda)$) can then be calculated and quantified as the difference (Δ) and relative difference (%) between total-band and in-band reflectance contributions. Because $\rho_{wN}(\lambda)$ spectra are generally a smooth function of the wavelength compared to those of $nL_w(\lambda)$, we use $\rho_{wN}(\lambda)$ spectra for computing sensor OOB effects. Thus, we can define the OOB (Δ) (difference) and OOB (%) (relative difference) in $\rho_{wN}(\lambda)$ as following:

$$OOB(\lambda_i)(\Delta) = \rho_{wN}^{(Total)}(\lambda_i) - \rho_{wN}^{(In\text{-}Band)}(\lambda_i) \tag{5}$$

and

$$OOB(\lambda_i)(\%) = \frac{OOB(\lambda_i)(\Delta)}{\rho_{wN}^{(In\text{-}Band)}(\lambda_i)} \times 100. \tag{6}$$

Alternatively, we can approximate the sensor OOB effects by relating the total-band $\rho_{wN}(\lambda)$ (Eq. (3)) to its value at the sensor nominal center wavelength $\lambda_i^{(N)}$, $\rho_{wN}\left(\lambda_i^{(N)}\right)$, i.e.,

$$OOB^{(N)}(\lambda_i)(\Delta) = \rho_{wN}^{(Total)}(\lambda_i) - \rho_{wN}\left(\lambda_i^{(N)}\right) \tag{7}$$

and

$$OOB^{(N)}(\lambda_i)(\%) = \frac{OOB^{(N)}(\lambda_i)(\Delta)}{\rho_{wN}\left(\lambda_i^{(N)}\right)} \times 100. \tag{8}$$

Furthermore, following *Wang et al.* (2001) [21], we can define a correction/conversion factor $Corr(\lambda_i)$ that converts the total-band normalized water-leaving reflectance $\rho_{wN}^{(Total)}(\lambda_i)$ in Eq. (3) to its value at the sensor nominal center wavelength $\lambda_i^{(N)}$, $\rho_{wN}\left(\lambda_i^{(N)}\right)$, i.e.,

$$Corr(\lambda_i) = \rho_{wN}\left(\lambda_i^{(N)}\right) \Big/ \rho_{wN}^{(Total)}(\lambda_i) \tag{9}$$

with $Corr(\lambda_i) = 1$ as no OOB effect. In fact, the value of $\rho_{wN}\left(\lambda_i^{(N)}\right)(1/Corr(\lambda_i) - 1)$ is the same as $OOB^{(N)}(\lambda_i)(\Delta)$ in Eq. (7), and $(1/Corr(\lambda_i) - 1)\times 100$ is the same as $OOB^{(N)}(\lambda_i)(\%)$ in Eq. (8). In practice, this conversion is quite useful as $\rho_{wN}(\lambda)$ at a specific wavelength can be derived and compared to the in situ data at the same wavelength (or to understand their differences). In addition, using this approach, satellite-measured $\rho_{wN}(\lambda)$ spectra can be converted to the same wavelength as from in situ measurements. It is noted that the multi-spectral in situ optics instrument also has SRFs. In this study, we calculate values of $OOB(\lambda_i)(\Delta)$, $OOB(\lambda_i)(\%)$, $OOB^{(N)}(\lambda_i)(\Delta)$, $OOB^{(N)}(\lambda_i)(\%)$, and $Corr(\lambda_i)$ for SeaWiFS, MODIS, and VIIRS.

It is noted that for multiple $\rho_{wN}(\lambda)$ spectra data from in situ measurements (i.e., MOBY and various coastal and inland waters), averages of $\langle OOB(\lambda_i)(\Delta)\rangle$ (or $\langle OOB^{(N)}(\lambda_i)(\Delta)\rangle$), $\langle OOB(\lambda_i)(\%)\rangle$ (or $\langle OOB^{(N)}(\lambda_i)(\%)\rangle$), and $\langle Corr(\lambda_i)\rangle$ are computed for the three satellite sensors based on the following equations:

$$\left\langle OOB(\lambda_i)(\Delta)\right\rangle = \left\langle \rho_{wN}^{(Total)}(\lambda_i) - \rho_{wN}^{(In\text{-}Band)}(\lambda_i)\right\rangle, \tag{10}$$

$$\left\langle OOB(\lambda_i)(\%)\right\rangle = \frac{\left\langle OOB(\lambda_i)(\Delta)\right\rangle}{\left\langle \rho_{wN}^{(In\text{-}Band)}(\lambda_i)\right\rangle} \times 100, \tag{11}$$

and

$$\left\langle Corr(\lambda_i)\right\rangle = \left\langle \rho_{wN}\left(\lambda_i^{(N)}\right) \Big/ \rho_{wN}^{(Total)}(\lambda_i)\right\rangle. \tag{12}$$

In particular, for computing $\langle OOB(\lambda_i)(\%)\rangle$ in Eq. (11), mean values of $OOB(\lambda_i)(\Delta)$ and $\rho_{wN}^{(In\text{-}Band)}(\lambda_i)$ are first calculated separately. The ratio of the two is then computed for the mean $\langle OOB(\lambda_i)(\%)\rangle$ to avoid the over-estimation of the impact with extremely low reflectance value on the mean difference (%) values. The same Eq. (10) and Eq. (11) (replacing $\rho_{wN}^{(In\text{-}Band)}(\lambda_i)$ with $\rho_{wN}\left(\lambda_i^{(N)}\right)$) are used for $<OOB^{(N)}(\lambda_i)(\Delta)>$ and $<OOB^{(N)}(\lambda_i)(\%)>$ computations, respectively.

We restrict our analysis of the OOB effects to the visible spectrum region for open oceans, as most in situ radiance measurements do not extend beyond this region, i.e., $\rho_{wN}(\lambda)$ spectra beyond the visible. This assumes that $\rho_{wN}(\lambda)$ spectra in the near-infrared (NIR) and shortwave infrared (SWIR) wavelengths are negligible. On the other hand, for turbid coastal and inland waters, $\rho_{wN}(\lambda)$ (or $nL_w(\lambda)$) contributions at the NIR and even SWIR wavelengths are important [17, 33, 34, 40, 41]. However, because the sensor SRF data (Fig. 2) do not cover the SWIR bands (or their $S_i(\lambda)$ contributions at the SWIR are negligible), the SWIR $\rho_{wN}(\lambda)$ contributions are effectively not included in this study. Although we have analyzed the spectral bandpass effects in $\rho_{wN}(\lambda)$ for most ocean color satellite sensors, we focus on SeaWiFS, MODIS, and VIIRS (particularly VIIRS and its OOB performance compared with others) for the sake of brevity and also as these sensors represent the most widely used satellite ocean color sensors for routine global ocean color data production.

3. SENSOR OOB EFFECT

A. The OOB Effect for the Three Study Cases

Results of the OOB contributions for the three satellite ocean color sensors are shown in Tables 2–4. Tables 2(a), 2(b), and 2(c) are OOB results from the MM01 model with various Chl-a data for SeaWiFS, MODIS, and VIIRS, respectively. The columns 1 to 9 in Table 2 correspond to Chl-a value, nominal center wavelength $\lambda_i^{(N)}$, effective band center wavelength $\lambda_i^{(E)}$, wavelength difference $\Delta\lambda$, $OOB(\lambda_i)(\Delta)$, $OOB(\lambda_i)(\%)$, $OOB^{(N)}(\lambda_i)(\Delta)$, $OOB^{(N)}(\lambda_i)(\%)$, and $Corr(\lambda_i)$, respectively. The effective band center wavelength $\lambda_i^{(E)}$ will be introduced and discussed in the next section. The OOB contribution can be positive or negative depending on whether the spectral reflectance (or radiance) in the entire spectral region is larger or smaller than that from the in-band spectral reflectance (Eqs. (5) and (6)). However, it is noted that adding extra powers (photons) in Eq. (3) does not necessarily lead to a positive OOB effect in Eq. (5). This is like computing a weighted mean value. Adding a larger than the "mean" value increases the new "mean" value, while including a smaller than the "mean" value decreases the new mean.

The OOB contributions for each of the sensor spectral bands for a variety of water types (ranging from oligotrophic to eutrophic waters) can be determined using $\rho_{wN}(\lambda)$ values derived from the MM01 model [29] with Chl-a as the input. Results in Table 2 show that for Case-1 waters important OOB effects (from *OOB* (Δ) and *OOB* (%)) are for the SeaWiFS 555 and 670 nm bands, MODIS 412 nm band, and VIIRS 551 and 671 nm bands. It is noted that wavelengths from the sensor band specifications (Table 1) are usually different from the actual nominal center wavelengths (Table 2). The notable OOB contribution at the MODIS 412 nm band is due to the relatively large sensor response $S_i(\lambda)$ contribution from the wavelength ranging of ~450–570 nm to this band (Fig. 2(a)) (leading to negative bias OOB difference). Significant OOB contributions at both SeaWiFS and VIIRS green bands are due to $S_i(\lambda)$ contributions at the wavelengths of ~375 to ~525 nm (blue leakage) (Fig. 2(d)), leading to biased high (positive) reflectance values. Although the largest *OOB* (%) bias values were observed at the SeaWiFS 670 nm and VIIRS 671 nm bands for extremely clear waters (e.g., ~30–40% at Chl-a of 0.03 mg m^{-3}), their absolute values in *OOB* (Δ) are quite small (Tables 2(a) and 2(c)). The large *OOB* (%) contributions are due to some leakage of blue light at SeaWiFS and VIIRS red bands (Fig. 2(e)), but mainly because of small red $\rho_{wN}(\lambda)$ values for open oceans (so percent change is high). It should be particularly noted that the important OOB contributions in the green bands (555 nm for SeaWiFS and 551 nm for VIIRS) have a significant effect on the satellite-derived Chl-a for clear (low Chl-a) oceanic waters [21], as $\rho_{wN}(\lambda)$ (or $nL_w(\lambda)$) in the green band is critical for deriving Chl-a data [8, 24]. Based on results from the MM01 model, VIIRS and SeaWiFS have a significant OOB contribution at the green band for low Chl-a values (~2–10%). In fact, it can be shown that [42], for the Chl-a algorithm based on blue/green reflectance ratio [8], error in Chl-a (*Δ*Chl-a) is proportional to the error difference between $\rho_{wN}(\lambda)$ at green band and blue band, i.e.,

$$\Delta Chl\text{-}a \propto \Delta\rho_{wN}(Green) - \Delta\rho_{wN}(Blue), \tag{13}$$

where $\Delta\rho_{wN}(Green)$ and $\Delta\rho_{wN}(Blue)$ are reflectance errors (or differences) at the green and blue band, respectively. Thus, it has been shown that, with SeaWiFS OOB green/blue reflectance difference in Eq. (13) about 3% for open oceans (Chl-a of 0.1 mg m^{-3}), it leads to biased high SeaWiFS Chl-a values for open oceans if uncorrected [21]. VIIRS has similar results as those from SeaWiFS, while MODIS has negligible OOB effect on the derived Chl-a data.

Table 3 shows results of the OOB effect for SeaWiFS, MODIS, and VIIRS derived from the in situ MOBY hyperspectral reflectance measurements. In situ MOBY $\rho_{wN}(\lambda)$ data (~4000 spectra data) are used for the OOB effect analysis (mean OOB values derived using Eqs. (10)–(12)) (Table 3). For the MOBY Hawaii site (oligotrophic waters), the OOB contribution is small for most wavebands except for 555 and 670 nm for SeaWiFS, 412 nm for MODIS, and 551 and 671 nm for VIIRS (Table 3). These results are generally comparable to results derived using the MM01 model for Chl-a of ~0.03–0.1 mg m^{-3} (Tables 2 and 3), showing that the MM01 model can be used to well predict and calculate the OOB contributions of various sensor wavebands in oligotrophic waters. Again, SeaWiFS and VIIRS have similar OOB performance from the MOBY in situ data.

Tables 4(a), 4(b), and 4(c) provide results for the OOB effect for SeaWiFS, MODIS, and VIIRS derived from in situ $\rho_{wN}(\lambda)$ measurements for three coastal and inland waters, i.e., the Chesapeake Bay (CB) [32], East China Sea (ECS) [33], and inland Lake Taihu [17, 34]. Results in Table 4(a) show that SeaWiFS has generally negligible OOB effects for the three coastal and inland water cases. In fact, the OOB effect (*OOB* (%)) for all SeaWiFS bands is less than 1% (the maximum is –0.99% for 555 nm band with the CB case). The *OOB* (Δ) values for SeaWiFS in the three Case-2 waters are also mostly negligible in the order of ~10^{-5}. For MODIS, the *OOB* (%) values for the three Case-2 waters are also quite small except for the 412 nm band ranging from 1.5 to ~3% (Table 4(b)). The *OOB* (Δ) values for MODIS are also quite small except for the 412 nm band with the maximum *OOB* (Δ) of ~10^{-3} for the case of Lake Taihu. The VIIRS

OOB performance for the three coastal and inland waters is similar to SeaWiFS (as for Case-1 waters in Tables 2 and 3), with its OOB effect within ~1% (Table 4(c)).

In summary, results in Tables 2–4 show that for Case-1 waters (from both the model MM01 and MOBY in situ data), the OOB effect is important for SeaWiFS 555 nm band, MODIS 412 nm band, and VIIRS 551 bands. SeaWiFS and VIIRS red bands have some notable OOB effects, but these differences are not important for oligotrophic waters (as reflectance values are very small). VIIRS has similar sensor OOB performance as SeaWiFS. On the other hand, for Case-2 waters with in situ $\rho_{wN}(\lambda)$ data from the CB, ECS, and Lake Taihu, the OOB effect is generally not that important for all three satellite sensors. There are some slight OOB effects for MODIS 412 nm band (~2–3%), SeaWiFS 555 nm band (within ~ −1%), and VIIRS 551 nm band (~ −1%).

B. The MM01 Model for the OOB Effect Correction

The OOB effect on the $\rho_{wN}(\lambda)$ (or $nL_w(\lambda)$) at nominal center wavelengths can be analyzed by computing $OOB^{(N)}(\lambda_i)(\Delta)$ (Eq. (7)) and $OOB^{(N)}(\lambda_i)(\%)$ (Eq. (8)), and by taking a ratio of the reflectance at nominal center wavelength to the total-band averaged reflectances, i.e., the OOB correction factor for ocean color data processing [21], which is indicated as "*Corr*" (Eq. (9)) in Tables 2–4. The correction factors of less than 1 indicate an overestimation in $\rho_{wN}(\lambda)$ at the nominal center wavelength compared to the corresponding total-band reflectance (i.e., values of $OOB^{(N)}(\Delta)$ and $OOB^{(N)}(\%) > 0$), while correction factor values greater than 1 indicate an underestimation (i.e., values of $OOB^{(N)}(\Delta)$ and $OOB^{(N)}(\%) < 0$). Consistent with results in *OOB* (Δ) and *OOB* (%), Tables 2–3 show that for Case-1 waters most important correction factors are for the SeaWiFS 555 nm band, MODIS 412 nm band, and VIIRS 551 nm band. Using the nominal center wavelength as a reference, the SeaWiFS 510 nm band also has significant OOB effect for highly clear ocean waters, showing large values in $OOB^{(N)}(\Delta)$ and $OOB^{(N)}(\%)$, as well as large correction *Corr* values (deviation from 1) (Tables 2(a) and 3). As expected, $OOB^{(N)}(\Delta)$ and $OOB^{(N)}(\%)$ values are generally larger than $OOB(\Delta)$ and $OOB(\%)$ due to sensor in-band SRF contributions, e.g., SeaWiFS 510 nm band also has significant in-band spectral variation. For coastal and inland waters, correction factors are all close to 1 with mostly negligible $OOB^{(N)}(\Delta)$ values for the three sensors (Table 4), although MODIS 412 nm band shows some slight effect, i.e., *Corr* values ~0.95–0.98 and $OOB^{(N)}(\Delta)$ values up to ~10^{-3} (Table 4(b)).

For satellite ocean color data processing, the OOB effects on $\rho_{wN}(\lambda)$ (or $nL_w(\lambda)$) can be corrected/converted to $\rho_{wN}(\lambda)$ at the sensor nominal center wavelengths using the MM01 model for the open ocean region [20, 21] with the correction factor described in Eq. (9) and results presented in the column "*Corr*" in Tables 2 and 3. It should be noted that the correction applied can be based on the MM01 model and hence assumes a Case-1 $\rho_{wN}(\lambda)$ spectral dependency. Obviously, the correction factor depends on the phytoplankton pigment concentration (Chl-a). Particularly for SeaWiFS 555 nm band and VIIRS 551 nm band, large correction factors are shown for cases with very clear ocean waters [21], i.e., lower Chl-a values with high blue to green reflectance ratio (Tables 2(a), 2(b), and 3). Since the *Wang et al.* (2001) [21] OOB correction methodology developed for SeaWiFS can be applied to other satellite ocean color sensors, the correction algorithm can be also used for VIIRS, particularly SeaWiFS and VIIRS have similar sensor OOB performance.

Indeed, following the *Wang et al.* (2001) [21] approach, Fig. 3 shows results of the OOB correction factor as a function of VIIRS-measured blue-green $nL_w(\lambda)$ (total band) ratio (i.e., $nL_w^{(Total)}(443)/nL_w^{(Total)}(551)$) for VIIRS spectral bands of 410, 443, 486, and 551 nm using the MM01 model (Case-1 waters). It is noted that different from the *Wang et al.* (2001) approach [21], the correction factor is now fitted with x-axis in the log-scale instead of linear scale. Much better fitting results are achieved with expanded coverage in $nL_w^{(Total)}(443)/nL_w^{(Total)}(551)$ ratio values, compared with those from *Wang et al.* (2001) [21]. Specifically, as shown in Fig. 3, we can derive best fittings with

$$Y = a_0 + a_1 \log(X) + a_2 [\log(X)]^2, \qquad (14)$$

where Y is the OOB correction factor and X is the blue-green normalized water-leaving radiance ratio $nL_w^{(Total)}(443)\big/nL_w^{(Total)}(551)$, with a_0, a_1, and a_2 the best fitting coefficients. The corresponding Chl-a values for the fittings in Fig. 3 are 0.01, 0.03, 0.1, 0.5, 1.0, 3.0, and 10.0 mg m^{-3} using the MM01 model [29]. The fitting coefficients a_0, a_1, and a_2 for VIIRS bands at 410, 443, 486, and 551 nm are also shown in Fig. 3. Specifically, the best fitting coefficients (a_0, a_1, a_2) for VIIRS spectral bands at 410, 443, 486, and 551 nm are (0.9975, 0.0104, 0.0275), (0.9975, 0.0211, 0.0012), (1.0061, 0.0231, –0.0142), and (0.9945, –0.0731, –0.0403), respectively.

Furthermore, it is useful to test these OOB corrections (e.g., Eq. (14) and Fig. 3), which are derived from Case-1 waters, for the applications over turbid coastal and inland waters. In particular, we need to understand if such OOB corrections lead to biased errors over turbid coastal and inland waters in satellite ocean color data processing. Figure 4 provides VIIRS results of the OOB correction factors derived from the correction formula Eq. (14) (Fig. 3) in comparison with those of true values from three turbid coastal and inland waters. The modeled correction factor values (y-axis) in Fig. 4 are derived from the fitting formula Eq. (14), while the measured correction factor values (x-axis) are computed from in situ data using Eq. (9) (as true values). Figures 4(a), 4(c), and 4(e) are results for VIIRS 443 nm band, while Figs. 4(b), 4(d), and 4(f) are comparison results for VIIRS 551 nm band. They are for cases over the Chesapeake Bay (Figs. 4(a) and 4(b)), East China Sea (Figs. 4(c) and 4(d)), and inland Lake Taihu (Figs. 4(e) and 4(f)). As discussed previously, for Case-1 waters VIIRS has negligible OOB effect for 443 nm, but with significant OOB contributions for the green band 551 nm. Results in Fig. 4 show that the OOB correction factor values are different from different coastal/inland waters (as expected) due to different $\rho_{wN}(\lambda)$ (or $nL_w(\lambda)$) spectral distributions (Fig. 1). Although there are some outliers for the correction factor in Fig. 4, overall the VIIRS OOB correction using Eq. (14) derived from Case-1 waters has not introduced noticeable errors in $nL_w(\lambda)$ for coastal and inland waters, i.e., errors in the OOB correction factor are generally negligible for the three examples of

Case-2 waters. In fact, the mean ratio values (indicated in Fig. 4) between the modeled and measured correction factors are all within 1%.

4. EFFECTIVE BAND CENTER WAVELENGTHS

It has been shown that significant OOB contribution often results in an increase or decrease in observed $\rho_{wN}(\lambda)$ above the measurement at the nominal center wavelength (Tables 2–4). Effectively, the OOB effect in $\rho_{wN}(\lambda)$ can be considered as the band center wavelength shifted in $\rho_{wN}(\lambda)$ from the nominal center wavelength (in optics/radiometric responses) without applying corrections for the OOB effect. For a given water property, the shift in the band center wavelengths due to the spectral band pass effects (i.e., the effective band center wavelengths) can be determined by comparing the total-band averaged $\rho_{wN}^{(Total)}(\lambda_i)$ (Eq. (3)) to $\rho_{wN}(\lambda)$ measured at an individual wavelength from hyperspectral $\rho_{wN}(\lambda)$ data, i.e.,

$$\rho_{wN}\left(\lambda_i^{(E)}\right) = \rho_{wN}^{(Total)}\left(\lambda_i\right), \tag{15}$$

where $\lambda_i^{(E)}$ is the effective band center wavelength for spectral band λ_i. Obviously, the effective band center wavelengths not only depend on the sensor SRF, but also on the measured water $\rho_{wN}(\lambda)$ spectra (target optics) (through Eqs. (1) and (3)). Theoretically, one can find $\lambda_i^{(E)}$ that satisfies Eq. (15) exactly. In practice, however, for a given water type with hyperspectral $\rho_{wN}(\lambda)$ spectra data, we compute the corresponding $\lambda_i^{(E)}$ using the following method: the $\lambda_i^{(E)}$ should correspond to the smallest wavelength shift from the nominal center wavelength with the small enough absolute reflectance difference between the two side of Eq. (15), i.e.,

$$\left|\rho_{wN}^{(Total)}\left(\lambda_i\right) - \rho_{wN}\left(\lambda_i^{(E)}\right)\right| \leq 5 \times 10^{-5}. \tag{16}$$

The reflectance difference 5×10^{-5} is about two-order smaller than the required atmospheric correction accuracy at visible bands for clear open oceans [18, 22, 23]. It is noted that with increase of the wavelength shift $\Delta\lambda$ from the nominal center wavelength $\lambda_i^{(N)}$, one may find smaller reflectance difference. However, this is not necessary due to other much large uncertainties from ocean color data processing (e.g., calibration, atmospheric correction, etc.). The effective band center wavelengths for SeaWiFS, MODIS, and VIIRS for various water cases are provided in Tables 2–4 (in the column $\lambda_i^{(E)}$). The $\lambda_i^{(E)}$ values are calculated corresponding to the various Case-1 and Case-2 waters using Eq. (16).

Results show that, for clear and turbid waters, the effective band center wavelengths are all within ±7 nm of the nominal center wavelengths except for SeaWiFS and VIIRS red bands. Consistent with results from previous analyses, large band shift $\Delta\lambda$ values are for SeaWiFS and VIIRS green bands and MODIS short blue band, and for extremely low Chl-a waters (Tables 2 and 3). For the satellite ocean color product validation purpose, one would prefer to have the same (or close) effective band center wavelength for both satellite sensor and in situ instrument for a specific water, to avoid measurement differences caused by different instrument characteristics (i.e., spectral band pass effects).

Therefore, for SeaWiFS 555 nm band, the OOB effect causes its effective band center wavelength $\lambda_i^{(E)}$ changing to (from nominal center wavelength of 555 nm) 548.4, 550.1, 552.1, 554.5, and 552.1 nm, corresponding to waters with Chl-a values of 0.01, 0.03, 0.1, 1.0, and 10.0 mg m^{-3}, respectively. In fact, Chl-a values can be replaced with blue/green reflectance ratio, as shown in the work by *Wang et al.* (2001) [21]. For MODIS 412 nm band, the corresponding effective band center wavelengths $\lambda_i^{(E)}$ are 417.7, 417.1, 415.6, 412.5, and 409.1 nm for Case-1 waters with Chl-a values of 0.01, 0.03, 0.1, 1.0, and 10.0 mg m^{-3}, respectively. VIIRS has a similar OOB performance as SeaWiFS, and its green band (551 nm) effective band center wavelengths are 546.1, 547.1, 547.6, 549.3, and 548.1 nm, respectively, for Case-1 waters with Chl-a values of 0.01, 0.03, 0.1, 1.0, and 10.0 mg m^{-3}, respectively.

It should be noted that, with hyperspectral in situ reflectance measurements, the sensor OOB effects can be accurately accounted for using Eq. (1) (or Eq. (3)) with $nL_w(\lambda)$ (or $\rho_{wN}(\lambda)$) from in situ hyperspectral data. Sensor SRF weighted in situ data (Eq. (1) or (3)) can then be compared with those from satellite measurements directly (for all different satellite sensors), i.e., no OOB correction is required. In this sense, hyperspectral in situ measurements are preferred for the purpose of accurately validating satellite-measured $nL_w(\lambda)$ spectra data.

5. CONCLUSION

In this paper, we analyzed in detail the spectral response function (bandpass) effects of ocean color satellite sensors SeaWiFS, MODIS, and VIIRS on the derived $\rho_{wN}(\lambda)$ (or $nL_w(\lambda)$) for open oceans and coastal/inland waters using the MM01 model and in situ data. For SeaWiFS and VIIRS, we found that for oligotrophic waters the OOB contribution is low for blue bands, whereas it is important for the green bands. The MODIS OOB effect is quite low except for the short blue band at 412 nm. The open ocean reflectance MM01 model provides reasonable estimations for the OOB contribution and correction factors for the in situ cases studied, showing consistent results with MOBY in situ data. Furthermore, results from this study show that the sensor OOB performance of VIIRS is similar to SeaWiFS. Hence, the same correction procedures developed for SeaWiFS can be implemented effectively for VIIRS. In fact, the formula for the VIIRS OOB correction factor has been derived and can be easily implemented. Results from this study also show that the sensor OOB effect for coastal and inland waters is generally negligible (from the three cases studied). Furthermore, using the VIIRS OOB correction formula, which is derived from Case-1 waters, does not lead to noticeable biased errors for the application in coastal and inland waters. Therefore, the *Wang et al.* (2001) sensor OOB correction approach, as well as the specific scheme developed in this study, can generally be used for global ocean color data processing. It should be noted that for the NASA satellite ocean color data processing the OOB correction has been applied.

Results from this study highlight the importance of the sensor spectral OOB response, especially in comparisons of ocean color data from different satellite sensors even though their nominal center wavelengths are identical. In addition, in order to accurately account for the satellite sensor OOB effects, hyperspectral in situ optics measurements are preferred for the satellite ocean color validation purpose. This study reiterates the importance of complete prelaunch sensor calibration and characterization, as well as such data available to the science community, on the quality of ocean color data product [19].

Acknowledgments

This work was supported by the NOAA Joint Polar Satellite System (JPSS) funding. We thank the MOBY team for providing the in situ data. We are grateful to all of the scientists and investigators who have contributed valuable in situ data to SeaBASS database and the NASA Ocean Biology Processing Group for maintaining and distributing the SeaBASS database. We thank Drs. Junwu Tang and Yunlin Zhang for the in situ data over turbid waters. The views, opinions, and findings contained in this paper are those of the authors and should not be construed as an official NOAA or U.S. Government position, policy, or decision.

References

1. H. R. Gordon, D. K. Clark, J. L. Mueller, and W. A. Hovis, “Phytoplankton Pigments from the Nimbus-7 Coastal Zone Color Scanner: Comparisons with Surface Measurements,” Science, 210, 63–66 (1980).
2. W. A. Hovis, D. K. Clark, F. Anderson, R. W. Austin, W. H. Wilson, E. T. Baker, D. Ball, H. R. Gordon, J. L. Mueller, S. T. E. Sayed, B. Strum, R. C. Wrigley, and C. S. Yentsch, “Nimbus 7 Coastal Zone Color Scanner: system description and initial imagery,” Science, 210, 60–63 (1980).
3. C. R. McClain, G. C. Feldman, and S. B. Hooker, “An overview of the SeaWiFS project and strategies for producing a climate research quality global ocean bio-optical time series,” Deep Sea Res. Part II, 51, 5–42 (2004).
4. W. E. Esaias, M. R. Abbott, I. Barton, O. B. Brown, J. W. Campbell, K. L. Carder, D. K. Clark, R. L. Evans, F. E. Hodge, H. R. Gordon, W. P. Balch, R. Letelier, and P. J. Minnet, “An overview of MODIS capabilities for ocean science observations,” IEEE Trans. Geosci. Remote Sens., 36, 1250–1265 (1998).
5. M. Rast, J. L. Bezy, and S. Bruzzi, “The ESA Medium Resolution Imaging Spectrometer MERIS a review of the instrument and its mission,” Int. J. Remote Sens., 20, 1681–1702 (1999).
6. M. D. Goldberg, H. Kilcoyne, H. Cikanek, and A. Mehta, “Joint Polar Satellite System: The United States next generation civilian polar-orbiting environmental satellite system,” J. Geophys. Res. Atmos., 118, 13463–13475 (2013).
7. M. Wang, X. Liu, L. Tan, L. Jiang, S. Son, W. Shi, K. Rausch, and K. Voss, “Impact of VIIRS SDR performance on ocean color products,” J. Geophys. Res. Atmos., 118, 10347–10360 (2013).

8. J. E. O'Reilly, S. Maritorena, B. G. Mitchell, D. A. Siegel, K. L. Carder, S. A. Garver, M. Kahru, and C. R. McClain, “Ocean color chlorophyll algorithms for SeaWiFS,” J. Geophys. Res., 103, 24937–24953 (1998).
9. Z. P. Lee, K. Du, and R. Arnone, “A model for the diffuse attenuation coefficient of downwelling irradiance,” J. Geophys. Res., 110, C02016, doi:10.1029/2004JC002275 (2005).
10. A. Morel, Y. Huot, B. Gentili, P. J. Werdell, S. B. Hooker, and B. A. Franz, “Examining the consistency of products derived from various ocean color sensors in open ocean (Case 1) waters in the perspective of a multi-sensor approach,” Remote Sens. Environ., 111, 69–88 (2007).
11. M. Wang, S. Son, and J. L. W. Harding, “Retrieval of diffuse attenuation coefficient in the Chesapeake Bay and turbid ocean regions for satellite ocean color applications,” J. Geophys. Res., 114, C10011, http://dx.doi.org/10.1029/2009JC005286 (2009).
12. M. J. Behrenfeld, R. T. O'Malley, D. A. Siegel, C. R. McClain, J. L. Sarmiento, G. C. Feldman, A. J. Milligan, P. G. Falkowski, R. M. Letelier, and E. S. Boss, “Climate-driven trends in contemporary ocean productivity,” Nature, 444, 752–755 (2006).
13. F. P. Chavez, P. G. Strutton, G. E. Friederich, R. A. Feely, G. C. Feldman, D. G. Foley, and M. J. McPhaden, “Biological and Chemical Response of the Equatorial Pacific Ocean to the 1997-98 El Niño,” Science, 286, 2126–2131 (1999).
14. C. R. McClain, “A decade of satellite ocean color observations,” Annual Review of Marine Science, 1, 19–42 (2009).
15. W. Shi, and M. Wang, “Satellite views of the Bohai Sea, Yellow Sea, and East China Sea,” Prog. Oceanogr., 104, 35–45 (2012).
16. S. Son, and M. Wang, “Water properties in Chesapeake Bay from MODIS-Aqua measurements,” Remote Sens. Environ., 123, 163–174 (2012).

17. M. Wang, W. Shi, and J. Tang, "Water property monitoring and assessment for China's inland Lake Taihu from MODIS-Aqua measurements," Remote Sens. Environ., 115, 841–854 (2011).
18. IOCCG, "Atmospheric Correction for Remotely-Sensed Ocean-Colour Products," Wang, M. (Ed.), *Reports of International Ocean-Colour Coordinating Group*, No. 10 (IOCCG, Dartmouth, Canada, 2010).
19. IOCCG, "Mission Requirements for Future Ocean-Colour Sensors," C. R. McClain and G. Meister (Eds.), *Reports of International Ocean-Colour Coordinating Group*, No. 13 (IOCCG, Dartmouth, Canada, 2012).
20. H. R. Gordon, "Remote sensing of ocean color: a methodology for dealing with broad spectral bands and significant out-of-band response," Appl. Opt., 34, 8363–8374 (1995).
21. M. Wang, B. A. Franz, R. A. Barnes, and C. R. McClain, "Effects of spectral bandpass on SeaWiFS-retrieved near-surface optical properties of the ocean," Appl. Opt., 40, 342–348 (2001).
22. H. R. Gordon, and M. Wang, "Retrieval of water-leaving radiance and aerosol optical thickness over the oceans with SeaWiFS: A preliminary algorithm," Appl. Opt., 33, 443–452 (1994).
23. M. Wang, "Remote sensing of the ocean contributions from ultraviolet to near-infrared using the shortwave infrared bands: simulations," Appl. Opt., 46, 1535–1547 (2007).
24. C. Hu, Z. Lee, and B. A. Franz, "Chlorophyll a algorithms for oligotrophic oceans: A novel approach based on three-band reflectance difference," J. Geophys. Res., 117, C01011, doi: 01010.01029/02011JC007395 (2012).
25. Z. P. Lee, K. L. Carder, and R. A. Arnone, "Deriving inherent optical properties from water color: a multiple quasi-analytical algorithm for optically deep waters," Appl. Opt., 41, 5755–5772 (2002).

26. S. Son, and M. Wang, “Diffuse attenuation coefficient of the photosynthetically available radiation Kd(PAR) for global open ocean and coastal waters,” Remote Sens. Environ., 159, 250–258 (2015).
27. S. W. Bailey, S. B. Hooker, D. Antoine, B. A. Franz, and P. J. Werdell, “Sources and assumptions for the vicarious calibration of ocean color satellite observations,” Appl. Opt., 47, 2035–2045 (2008).
28. H. R. Gordon, O. B. Brown, R. H. Evans, J. W. Brown, R. C. Smith, K. S. Baker, and D. K. Clark, “A semianalytic radiance model of ocean color,” J. Geophys. Res., 93, 10909–10924 (1988).
29. A. Morel, and S. Maritorena, “Bio-optical properties of oceanic waters: A reappraisal,” J. Geophys. Res., 106, 7163–7180 (2001).
30. B. A. Franz, J. R. E. Eplee, S. W. Bailey, and M. Wang, “Changes to the atmospheric correction algorithm and retrieval of oceanic optical properties,” (NASA Goddard Space Flight Center, Greenbelt, Maryland, 2003), pp. 29-33.
31. D. K. Clark, H. R. Gordon, K. J. Voss, Y. Ge, W. Broenkow, and C. Trees, “Validation of atmospheric correction over the ocean,” J. Geophys. Res., 102, 17209–17217 (1997).
32. P. J. Werdell, and S. W. Bailey, “An improved in-situ bio-optical data set for ocean color algorithm development and satellite data product validation,” Remote Sens. Environ., 98, 122–140 (2005).
33. M. Wang, J. Tang, and W. Shi, “MODIS-derived ocean color products along the China east coastal region,” Geophy. Res. Lett., 34, L06611, http://dx.doi.org/10.1029/2006GL028599 (2007).
34. M. Wang, S. Son, Y. Zhang, and W. Shi, “Remote sensing of water optical property for China's inland Lake Taihu using the SWIR atmospheric correction with 1640 and 2130 nm bands,” IEEE J. Sel. Topics Appl. Earth Observ. Remote Sens., 6, 2505–2516 (2013).

35. A. Morel, and G. Gentili, “Diffuse reflectance of oceanic waters. III. Implication of bidirectionality for the remote-sensing problem,” Appl. Opt., 35, 4850–4862 (1996).
36. H. R. Gordon, “Normalized water-leaving radiance: revisiting the influence of surface roughness,” Appl. Opt., 44, 241–248 (2005).
37. M. Wang, “Effects of ocean surface reflectance variation with solar elevation on normalized water-leaving radiance,” Appl. Opt., 45, 4122–4128 (2006).
38. S. Son, M. Wang, and L. W. Harding Jr., “Satellite-measured net primary production in the Chesapeake Bay,” Remote Sens. Environ., 144, 109–119 (2014).
39. G. Thuillier, M. Herse, D. Labs, T. Foujols, W. Peetermans, D. Gillotay, P. C. Simon, and H. Mandel, “The solar spectral irradiance from 200 to 2400 nm as measured by the SOLSPEC spectrometer from the ATLAS and EURECA missions,” Solar Physics, 214, 1–22 (2003).
40. W. Shi, and M. Wang, “Characterization of global ocean turbidity from Moderate Resolution Imaging Spectroradiometer ocean color observations,” J. Geophys. Res., 115, C11022, http://dx.doi.org/10.1029/2010JC006160 (2010).
41. W. Shi, and M. Wang, “Ocean reflectance spectra at the red, near-infrared, and shortwave infrared from highly turbid waters: A study in the Bohai Sea, Yellow Sea, and East China Sea,” Limnol. Oceanogr., 59, 427–444 (2014).
42. M. Wang, W. Shi, L. Jiang, X. Liu, S. Son, and K. Voss, “Technique for monitoring performance of VIIRS reflective solar bands for ocean color data processing,” Opt. Express, 23, 14446–14460 (2015).

Figure Captions

Figure 1. Examples of in situ normalized water-leaving reflectance $\rho_{wN}(\lambda)$ spectra as a function of the wavelength for waters over Hawaii MOBY site, the Chesapeake Bay, East China Sea, and inland Lake Taihu.

Figure 2. Spectral response functions as a function of wavelength for SeaWiFS, MODIS, and VIIRS for visible region bands.

Figure 3. Results of the OOB correction factor as a function of VIIRS-measured blue-green $nL_w(\lambda)$ (total band) ratio ($nL_w^{(Total)}(443)/nL_w^{(Total)}(551)$) for VIIRS spectral bands of 410, 443, 486, and 551 nm using the MM01 model.

Figure 4. VIIRS results of the OOB correction factors derived from the correction formula Eq. (14) in comparison with those of true values for VIIRS bands of 443 and 551 nm with the water region of (a) and (b) Chesapeake Bay, (c) and (d) East China Sea, and (e) and (f) Lake Taihu.

Table Captions

Table 1. Specifications of ocean color spectral bands for SeaWiFS, MODIS, and VIIRS.

Table 2. The nominal center wavelength ($\lambda_i^{(N)}$), effective band center wavelengths ($\lambda_i^{(E)}$), difference between the nominal center wavelength and effective band center wavelength $\Delta\lambda$, OOB contribution (*OOB* (Δ)) (Eq. (5)) and its relative OOB contribution (*OOB* (%)) (Eq. (6)), OOB contribution in reference to the nominal center wavelength $OOB^{(N)}(\Delta)$ (Eq. (7)) and the corresponding relative OOB contribution $OOB^{(N)}(\%)$ (Eq. (8)), and the OOB correction factor *Corr* (Eq. (9)) for Chl-a values of 0.03, 0.01, 0.1, 1.0, and 10 mg m^{-3} using the MM01 model for (a) SeaWiFS, (b) MODIS, and (c) VIIRS using the MM01 model.

Table 3. The nominal center wavelength ($\lambda_i^{(N)}$), effective band center wavelengths ($\lambda_i^{(E)}$), difference between the nominal center wavelength and effective band center wavelength $\Delta\lambda$, OOB contribution (*OOB* (Δ)) (Eq. (5)) and its relative OOB contribution (*OOB* (%)) (Eq. (6)),

OOB contribution in reference to the nominal center wavelength $OOB^{(N)}(\Delta)$ (Eq. (7)) and the corresponding relative OOB contribution $OOB^{(N)}(\%)$ (Eq. (8)), and the OOB correction factor *Corr* (Eq. (9)) using MOBY in situ data for SeaWiFS, MODIS, and VIIRS.

Table 4. The nominal center wavelength ($\lambda_i^{(N)}$), effective band center wavelengths ($\lambda_i^{(E)}$), difference between the nominal center wavelength and effective band center wavelength $\Delta\lambda$, OOB contribution (OOB (Δ)) (Eq. (5)) and its relative OOB contribution (OOB (%)) (Eq. (6)), OOB contribution in reference to the nominal center wavelength $OOB^{(N)}(\Delta)$ (Eq. (7)) and the corresponding relative OOB contribution $OOB^{(N)}(\%)$ (Eq. (8)), and the OOB correction factor *Corr* (Eq. (9)) from in situ coastal and inland waters in the CB, ECS, and Lake Taihu for (a) SeaWiFS, (b) MODIS, and (c) VIIRS.

Tables

Table 1. Specifications of ocean color spectral bands for SeaWiFS, MODIS, and VIIRS.

SeaWiFS (nm)	**MODIS** (nm)	**VIIRS** (nm)
412	412	412 (M1)
443	443	445 (M2)
490	488	488 (M3)
510	531	—
555	551	555 (M4)
670	667	672 (M5)
—	678	—
765	748	746 (M6)
865	869	865 (M7)

Table 2(a): The nominal center wavelength ($\lambda_i^{(N)}$), effective band center wavelengths ($\lambda_i^{(E)}$), difference between the nominal center wavelength and effective band center wavelength $\Delta\lambda$, OOB contribution (*OOB* (Δ)) (Eq. (5)) and its relative OOB contribution (*OOB* (%)) (Eq. (6)), OOB contribution in reference to the nominal center wavelength $OOB^{(N)}(\Delta)$ (Eq. (7)) and the corresponding relative OOB contribution $OOB^{(N)}(\%)$ (Eq. (8)), and the OOB correction factor *Corr* (Eq. (9)) for Chl-a values of 0.03, 0.01, 0.1, 1.0, and 10 mg m^{-3} using the MM01 model for (a) SeaWiFS, (b) MODIS, and (c) VIIRS using the MM01 model.

SeaWiFS								
Chl-a (mg/m^3)	$\lambda_i^{(N)}$ (nm)	$\lambda_i^{(E)}$ (nm)	$\Delta\lambda$ (nm)	***OOB* (Δ)**	***OOB* (%)**	$OOB^{(N)}(\Delta)$	$OOB^{(N)}(\%)$	***Corr***
0.01	413	417.1	-4.1	-2.39E-04	-0.309	-2.85E-03	-3.562	1.037
	444	443.9	0.1	1.40E-05	0.030	1.61E-04	0.346	0.997
	491	491.5	-0.5	-5.40E-05	-0.268	-2.73E-04	-1.340	1.014
	510	507.8	2.2	8.90E-05	0.876	1.21E-03	13.406	0.882
	555	548.4	6.6	3.90E-04	9.941	4.89E-04	12.788	0.887
	668	655.1	12.9	1.23E-04	48.425	1.21E-04	47.266	0.679
0.03	413	415.8	-2.8	-1.16E-04	-0.248	-8.73E-04	-1.835	1.019
	444	444.2	-0.2	2.00E-06	0.006	-1.37E-04	-0.406	1.004
	491	491.8	-0.8	-6.20E-05	-0.332	-3.54E-04	-1.867	1.019
	510	508.1	1.9	5.60E-05	0.542	1.02E-03	10.874	0.902
	555	550.1	4.9	2.41E-04	5.525	3.44E-04	8.077	0.925
	668	657.1	10.9	9.70E-05	29.938	9.60E-05	29.538	0.772
0.1	413	413.9	-0.9	-5.60E-05	-0.195	-2.45E-04	-0.847	1.009
	444	444.5	-0.5	0.00E+00	0.000	-9.00E-05	-0.395	1.004
	491	492.3	-1.3	-5.50E-05	-0.346	-3.42E-04	-2.112	1.022
	510	508.3	1.7	3.00E-05	0.300	7.25E-04	7.779	0.928
	555	552.1	2.9	1.29E-04	2.652	2.29E-04	4.806	0.954
	668	661.1	6.9	7.30E-05	16.859	7.30E-05	16.859	0.856
1.0	413	412.6	0.4	-4.00E-06	-0.037	3.50E-05	0.329	0.997
	444	444.9	-0.9	2.00E-06	0.020	3.40E-05	0.346	0.997
	491	496.9	-5.9	-2.50E-05	-0.232	-1.58E-04	-1.449	1.015
	510	509.1	0.9	-1.00E-06	-0.010	1.73E-04	1.836	0.982
	555	554.5	0.5	-3.50E-05	-0.460	2.30E-05	0.305	0.997
	668	667.1	0.9	4.10E-05	3.846	4.80E-05	4.533	0.957
10.0	413	412.1	0.9	7.00E-06	0.139	4.20E-05	0.841	0.992
	444	444.9	-0.9	4.00E-06	0.079	4.50E-05	0.900	0.991
	491	491.4	-0.4	1.50E-05	0.214	2.60E-05	0.372	0.996
	510	510.9	-0.9	-6.00E-06	-0.074	5.50E-05	0.685	0.993
	555	552.1	2.9	-1.37E-04	-1.170	-2.51E-04	-2.122	1.022
	668	667.1	0.9	2.50E-05	0.964	5.80E-05	2.265	0.978

Table 2(b): Same as Table 2(a), but for MODIS.

MODIS								
Chl-a (mg/m^3)	$\lambda_i^{(N)}$ (nm)	$\lambda_i^{(E)}$ (nm)	**Δλ** (nm)	***OOB* (Δ)**	***OOB* (%)**	***OOB*$^{(N)}$(Δ)**	***OOB*$^{(N)}$(%)**	***Corr***
0.01	412	417.7	-5.7	-1.94E-03	-2.476	-3.84E-03	-4.782	1.050
	442	442.3	-0.3	-1.33E-04	-0.272	-3.43E-04	-0.698	1.007
	488	487.4	0.6	7.60E-05	0.342	3.30E-04	1.502	0.985
	530	529.6	0.4	8.00E-06	0.133	3.70E-05	0.617	0.994
	547	546.8	0.2	2.10E-05	0.468	2.00E-05	0.445	0.996
	666	665.2	0.8	2.00E-06	0.769	4.00E-06	1.550	0.985
0.03	412	417.1	-5.1	-1.03E-03	-2.196	-1.74E-03	-3.635	1.038
	442	442.4	-0.4	-9.40E-05	-0.271	-2.34E-04	-0.672	1.007
	488	487.5	0.5	1.60E-05	0.079	1.73E-04	0.859	0.991
	530	529.7	0.3	6.00E-06	0.092	3.10E-05	0.480	0.995
	547	546.9	0.1	1.60E-05	0.323	1.40E-05	0.283	0.997
	666	665.2	0.8	3.00E-06	0.912	4.00E-06	1.220	0.988
0.1	412	415.6	-3.6	-5.32E-04	-1.843	-8.07E-04	-2.770	1.028
	442	442.6	-0.6	-5.50E-05	-0.238	-1.10E-04	-0.474	1.005
	488	487.7	0.3	-1.20E-05	-0.071	5.40E-05	0.320	0.997
	530	529.8	0.2	2.00E-06	0.029	1.80E-05	0.261	0.997
	547	547.0	0.0	1.10E-05	0.202	6.00E-06	0.110	0.999
	666	665.1	0.9	2.00E-06	0.456	4.00E-06	0.915	0.991
1.0	412	412.5	-0.5	-4.00E-05	-0.373	-4.10E-05	-0.382	1.004
	442	442.9	-0.9	-4.00E-06	-0.041	8.00E-06	0.082	0.999
	488	487.1	0.9	-1.80E-05	-0.166	-5.10E-05	-0.468	1.005
	530	530.4	-0.4	-4.00E-06	-0.045	-5.00E-06	-0.057	1.001
	547	547.2	-0.2	0.00E+00	0.000	-1.60E-05	-0.198	1.002
	666	665.1	0.9	2.00E-06	0.186	8.00E-06	0.747	0.993
10.0	412	409.1	2.9	1.01E-04	1.995	1.37E-04	2.725	0.973
	442	442.9	-0.9	1.80E-05	0.362	3.20E-05	0.646	0.994
	488	487.5	0.5	3.00E-06	0.044	-3.00E-05	-0.440	1.004
	530	530.2	-0.2	0.00E+00	0.000	2.10E-05	0.213	0.998
	547	546.9	0.1	-9.00E-06	-0.079	-7.00E-06	-0.062	1.001
	666	665.4	0.6	4.00E-06	0.153	1.20E-05	0.461	0.995

Table 2(c): Same as Table 2(a), but for VIIRS.

VIIRS								
Chl-a (mg/m^3)	$\lambda_i^{(N)}$ (nm)	$\lambda_i^{(E)}$ (nm)	$\Delta\lambda$ (nm)	***OOB*** **(Δ)**	***OOB*** **(%)**	$OOB^{(N)}(\Delta)$	$OOB^{(N)}$ **(%)**	***Corr***
0.01	410	416.4	-6.4	-4.43E-04	-0.566	-3.13E-03	-3.868	1.040
	443	443.7	-0.7	-1.39E-04	-0.295	-9.17E-04	-1.916	1.020
	486	486.6	-0.6	-7.40E-05	-0.325	-3.21E-04	-1.396	1.014
	551	546.1	4.9	3.86E-04	9.095	5.72E-04	14.096	0.876
	671	654.1	16.9	1.44E-04	58.776	1.39E-04	55.600	0.643
0.03	410	413.9	-3.9	-2.58E-04	-0.543	-1.07E-03	-2.212	1.023
	443	444.0	-1.0	-1.01E-04	-0.299	-5.81E-04	-1.695	1.017
	486	486.9	-0.9	-7.00E-05	-0.340	-3.31E-04	-1.586	1.016
	551	547.1	3.9	2.82E-04	6.008	4.72E-04	10.480	0.905
	671	656.1	14.9	1.22E-04	38.978	1.18E-04	37.224	0.729
0.1	410	411.7	-1.7	-1.54E-04	-0.525	-3.68E-04	-1.244	1.013
	443	444.3	-1.3	-6.60E-05	-0.289	-2.66E-04	-1.156	1.012
	486	487.3	-1.3	-5.80E-05	-0.340	-2.66E-04	-1.540	1.016
	551	547.6	3.4	1.80E-04	3.466	3.60E-04	7.180	0.933
	671	659.1	11.9	1.00E-04	23.753	9.70E-05	22.877	0.814
1.0	410	410.1	-0.1	-4.80E-05	-0.439	-1.20E-05	-0.110	1.001
	443	443.5	-0.5	-1.70E-05	-0.173	4.00E-06	0.041	1.000
	486	484.1	1.9	-2.80E-05	-0.259	-8.50E-05	-0.783	1.008
	551	549.3	1.7	9.99E-07	0.013	1.20E-04	1.550	0.985
	671	665.1	5.9	8.00E-05	7.678	8.00E-05	7.678	0.929
10.0	410	409.5	0.5	-7.00E-06	-0.137	2.50E-05	0.491	0.995
	443	443.9	-0.9	9.00E-06	0.179	4.70E-05	0.944	0.991
	486	486.4	-0.4	0.00E+00	0.000	2.00E-05	0.299	0.997
	551	548.1	2.9	-1.30E-04	-1.130	-1.76E-04	-1.524	1.015
	671	667.1	3.9	7.90E-05	3.105	1.16E-04	4.627	0.956

Table 3: The nominal center wavelength ($\lambda_i^{(N)}$), effective band center wavelengths ($\lambda_i^{(E)}$), difference between the nominal center wavelength and effective band center wavelength $\Delta\lambda$, OOB contribution (*OOB* (Δ)) (Eq. (5)) and its relative OOB contribution (*OOB* (%)) (Eq. (6)), OOB contribution in reference to the nominal center wavelength $OOB^{(N)}$(Δ) (Eq. (7)) and the corresponding relative OOB contribution $OOB^{(N)}$(%) (Eq. (8)), and the OOB correction factor *Corr* (Eq. (9)) using MOBY in situ data for SeaWiFS, MODIS, and VIIRS.

MOBY In Situ Data							
$\lambda_i^{(N)}$ (nm)	$\lambda_i^{(E)}$ (nm)	$\Delta\lambda$ (nm)	***OOB* (Δ)**	***OOB* (%)**	$OOB^{(N)}$**(Δ)**	$OOB^{(N)}$**(%)**	***Corr***
SeaWiFS							
413	414.4	-1.4	-8.14E-05	-0.221	-3.29E-04	-0.887	1.009
444	444.4	-0.4	2.87E-06	0.010	-1.32E-04	-0.475	1.005
491	492.3	-1.3	-6.36E-05	-0.359	-4.63E-04	-2.555	1.026
510	508.5	1.5	4.24E-05	0.410	8.16E-04	8.527	0.921
555	551.3	3.8	1.81E-04	4.253	2.88E-04	6.947	0.935
668	657.2	10.8	8.52E-05	31.957	8.84E-05	33.526	0.746
MODIS							
412	416.8	-4.8	-7.49E-04	-2.029	-9.88E-04	-2.659	1.027
442	442.3	-0.3	-7.33E-05	-0.259	-1.09E-04	-0.384	1.004
488	487.7	0.3	-7.66E-06	-0.040	1.04E-04	0.547	0.995
530	530.0	0.0	3.28E-06	0.049	-7.80E-07	-0.012	1.000
547	547.1	-0.1	1.44E-05	0.293	-5.98E-06	-0.122	1.001
666	665.9	0.1	1.86E-06	0.697	4.41E-06	1.670	0.983
VIIRS							
410	411.3	-1.3	-2.37E-04	-0.631	-6.88E-04	-1.815	1.018
443	444.3	-1.3	-9.52E-05	-0.344	-4.69E-04	-1.671	1.017
486	487.6	-1.6	-8.55E-05	-0.442	-8.69E-04	-4.322	1.045
551	547.8	3.3	2.25E-04	4.868	3.91E-04	8.797	0.919
671	656.5	14.5	1.09E-04	41.698	1.08E-04	41.385	0.704

Table 4(a): The nominal center wavelength ($\lambda_i^{(N)}$), effective band center wavelengths ($\lambda_i^{(E)}$), difference between the nominal center wavelength and effective band center wavelength $\Delta\lambda$, OOB contribution (*OOB* (Δ)) (Eq. (5)) and its relative OOB contribution (*OOB* (%)) (Eq. (6)), OOB contribution in reference to the nominal center wavelength $OOB^{(N)}$(Δ) (Eq. (7)) and the corresponding relative OOB contribution $OOB^{(N)}$(%) (Eq. (8)), and the OOB correction factor *Corr* (Eq. (9)) from in situ coastal and inland waters in the CB, ECS, and Lake Taihu for (a) SeaWiFS, (b) MODIS, and (c) VIIRS.

SeaWiFS									
Turbid Region	$\lambda_i^{(N)}$ (nm)	$\lambda_i^{(E)}$ (nm)	**Δλ** (nm)	***OOB* (Δ)**	***OOB* (%)**	**$OOB^{(N)}$(Δ)**	**$OOB^{(N)}$(%)**	***Corr***
CB	413	414.0	-1.0	1.76E-05	0.146	6.82E-05	0.568	0.993
	444	444.9	-0.9	2.56E-06	0.019	9.17E-05	0.683	0.992
	491	490.7	0.3	-2.10E-06	-0.012	-3.40E-05	-0.196	1.002
	510	510.0	0.0	-1.46E-05	-0.079	-3.56E-05	-0.193	1.002
	555	555.5	-0.5	-2.04E-04	-0.990	-1.88E-04	-0.910	1.008
	668	667.0	1.0	4.06E-05	0.557	1.48E-04	2.060	0.971
ECS	413	413.8	-0.8	5.94E-05	0.248	6.33E-04	2.708	0.967
	444	444.4	-0.4	1.94E-06	0.006	3.21E-05	0.106	1.000
	491	490.2	0.8	2.19E-05	0.054	-2.15E-04	-0.525	1.008
	510	510.2	-0.2	-3.42E-05	-0.079	1.69E-05	0.039	0.999
	555	555.0	0.0	-4.20E-04	-0.830	-3.22E-04	-0.637	1.007
	668	667.1	0.9	3.64E-05	0.128	2.14E-04	0.758	0.967
Lake Taihu	413	414.2	-1.2	1.08E-04	0.271	4.00E-04	1.015	0.990
	444	444.8	-0.8	1.05E-05	0.021	3.03E-04	0.608	0.991
	491	492.1	-1.1	1.36E-04	0.205	3.14E-04	0.476	0.995
	510	510.0	0.0	-4.58E-05	-0.061	7.82E-05	0.104	0.998
	555	552.5	2.5	-6.73E-04	-0.663	-1.21E-03	-1.182	1.012
	668	667.0	1.0	-1.52E-05	-0.019	8.03E-04	1.036	0.987

Table 4(b): Same as Table 4(a), but for MODIS.

MODIS								
Turbid Region	$\lambda_i^{(N)}$ (nm)	$\lambda_i^{(E)}$ (nm)	$\Delta\lambda$ (nm)	***OOB* (Δ)**	***OOB* (%)**	***OOB*$^{(N)}$(Δ)**	***OOB*$^{(N)}$(%)**	***Corr***
CB	412	417.0	-5.0	1.81E-04	1.504	2.56E-04	2.135	0.975
	442	442.7	-0.7	2.13E-05	0.160	6.49E-05	0.489	0.994
	488	487.1	0.9	-1.48E-05	-0.087	-9.08E-05	-0.529	1.006
	530	529.7	0.3	-5.42E-06	-0.027	-2.70E-05	-0.136	1.001
	547	547.2	-0.2	-9.21E-06	-0.045	-3.17E-05	-0.154	1.002
	666	665.7	0.3	-1.28E-05	-0.176	3.30E-05	0.457	1.027
ECS	412	414.1	-2.1	5.76E-04	2.411	1.01E-03	4.306	0.959
	442	442.2	-0.2	5.68E-05	0.191	2.29E-05	0.077	1.002
	488	487.2	0.8	-2.55E-05	-0.064	-3.17E-04	-0.786	1.008
	530	530.4	-0.4	8.47E-07	0.002	8.36E-05	0.180	0.999
	547	547.1	-0.1	-1.33E-05	-0.027	-4.53E-06	-0.009	1.001
	666	666.2	-0.2	-6.63E-05	-0.233	6.92E-05	0.244	0.988
Lake Taihu	412	417.0	-5.0	1.13E-03	2.858	1.57E-03	4.005	0.96
	442	442.8	-0.8	1.41E-04	0.286	3.04E-04	0.619	0.993
	488	487.6	0.4	3.14E-05	0.048	-1.56E-04	-0.240	1.002
	530	530.1	-0.1	4.72E-06	0.005	7.49E-05	0.085	0.999
	547	546.9	0.1	-5.91E-05	-0.060	-9.66E-05	-0.098	1.001
	666	666.4	-0.4	-1.25E-04	-0.158	1.18E-04	0.150	0.998

Table 4(c): Same as Table 4(a), but for VIIRS.

VIIRS								
Turbid Region	$\lambda_i^{(N)}$ (nm)	$\lambda_i^{(E)}$ (nm)	$\Delta\lambda$ (nm)	***OOB*** **(Δ)**	***OOB*** **(%)**	$OOB^{(N)}(\Delta)$	$OOB^{(N)}(\%)$	***Corr***
CB	410	410.0	0.0	-1.10E-04	-0.921	-9.18E-05	-0.770	1.008
	443	443.9	-0.9	-1.95E-05	-0.145	8.27E-05	0.620	0.993
	486	484.7	1.3	-7.44E-05	-0.439	-1.11E-04	-0.651	1.007
	551	548.4	2.6	-2.40E-04	-1.166	-1.93E-04	-0.938	1.009
	671	667.6	3.4	9.44E-05	1.300	1.56E-04	2.159	0.970
ECS	410	409.9	0.1	-1.06E-04	-0.452	-1.14E-04	-0.484	1.013
	443	443.3	-0.3	-9.25E-06	-0.031	2.22E-04	0.743	0.994
	486	484.6	1.4	-1.32E-04	-0.332	-1.20E-04	-0.303	1.006
	551	549.0	2.0	-5.10E-04	-1.023	-3.82E-04	-0.768	1.005
	671	670.6	0.4	7.91E-05	0.279	1.66E-04	0.588	0.964
Lake Taihu	410	411.3	-1.3	2.81E-04	0.719	5.54E-04	1.426	0.986
	443	444.4	-1.4	1.33E-04	0.267	5.90E-04	1.193	0.986
	486	486.6	-0.6	2.87E-05	0.044	1.60E-04	0.248	0.997
	551	547.5	3.5	-9.65E-04	-0.965	-1.57E-03	-1.560	1.016
	671	669.3	1.7	2.26E-05	0.029	1.07E-03	1.400	0.981

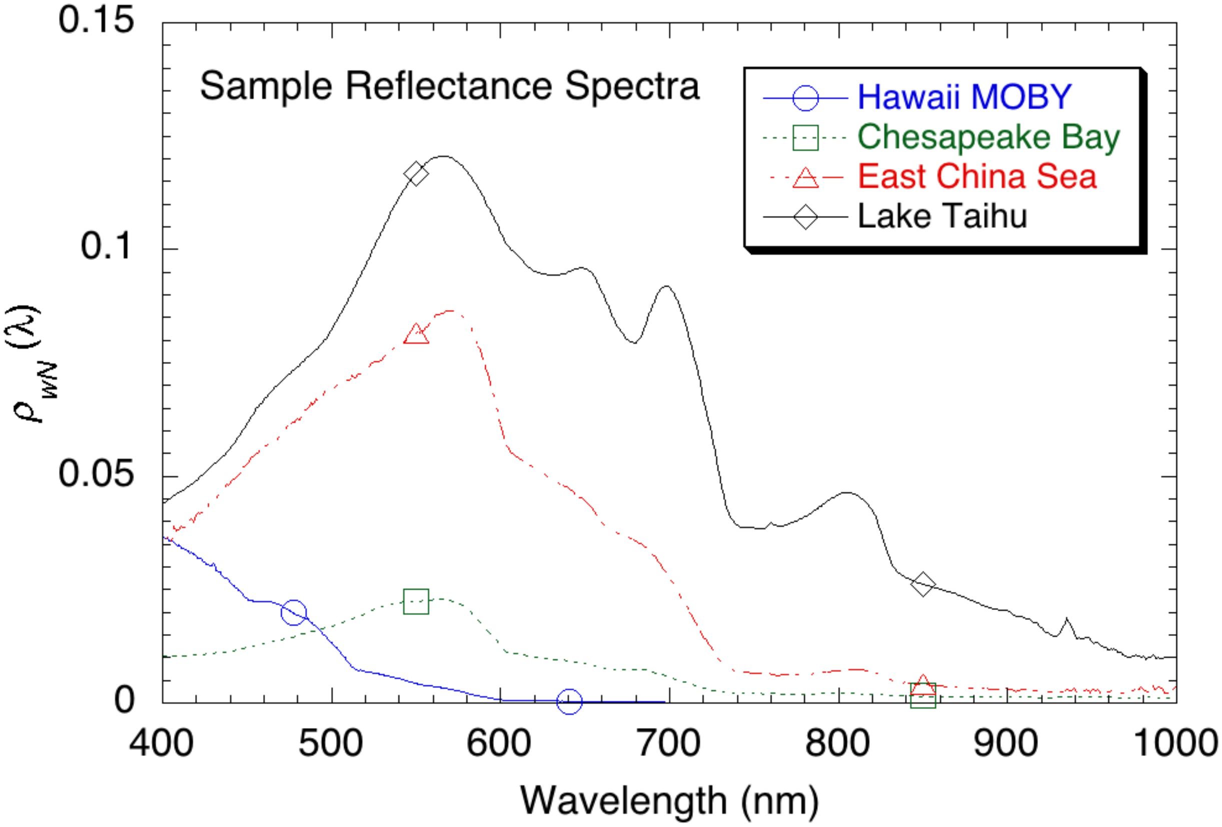

Figure 1. Examples of in situ normalized water-leaving reflectance $\rho_{wN}(\lambda)$ spectra as a function of the wavelength for waters over Hawaii MOBY site, the Chesapeake Bay, East China Sea, and inland Lake Taihu.

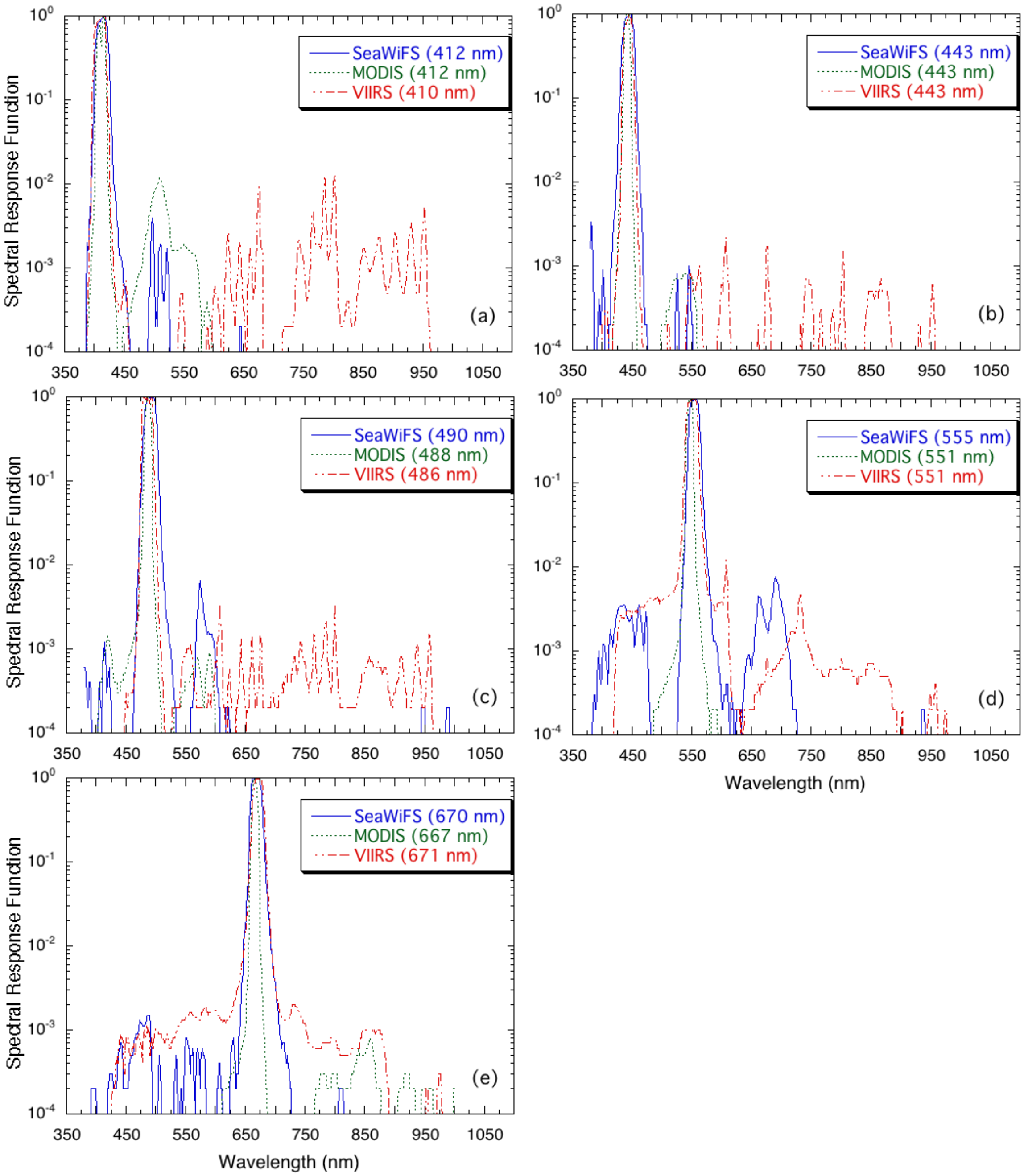

Figure 2. Spectral response functions as a function of wavelength for SeaWiFS, MODIS, and VIIRS for visible region bands.

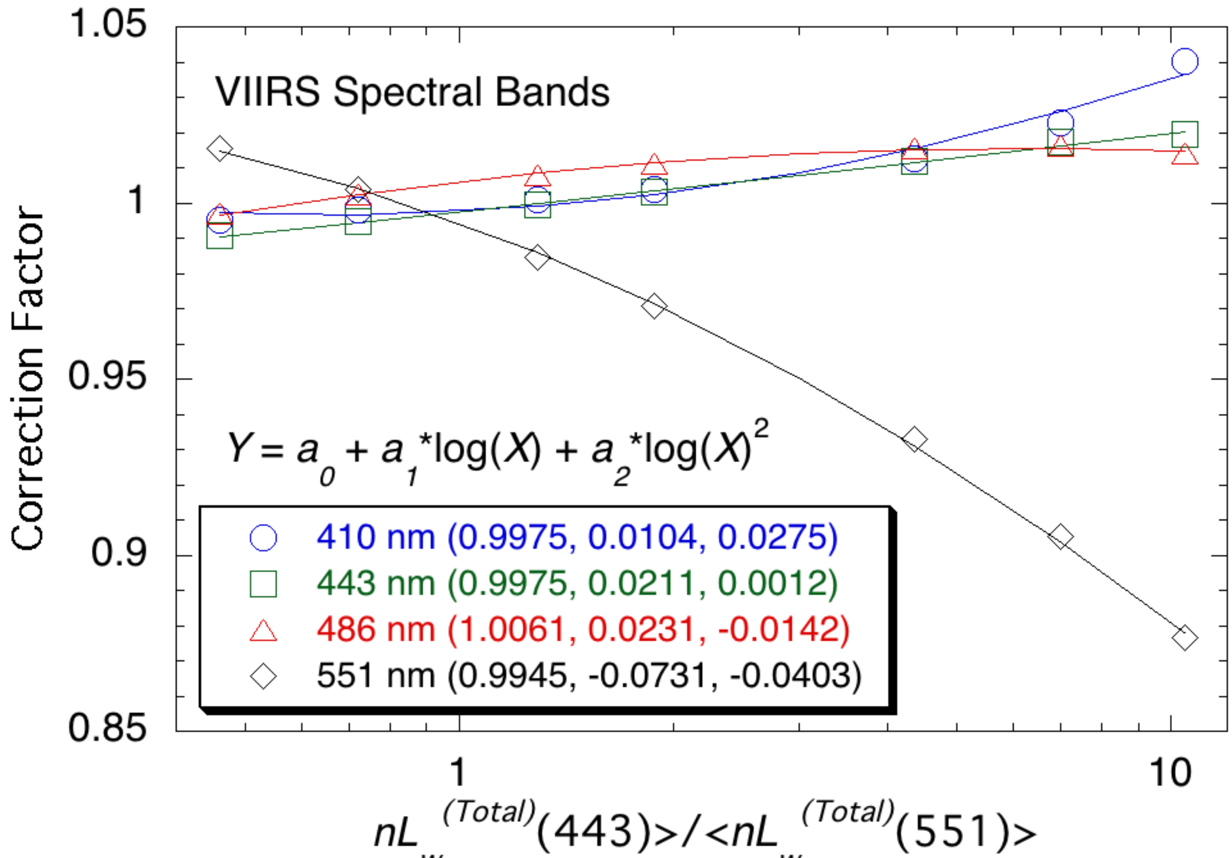

Figure 3. Results of the OOB correction factor as a function of VIIRS-measured blue-green $nL_w(\lambda)$ (total band) ratio ($nL_w^{(Total)}(443)/nL_w^{(Total)}(551)$) for VIIRS spectral bands of 410, 443, 486, and 551 nm using the MM01 model.

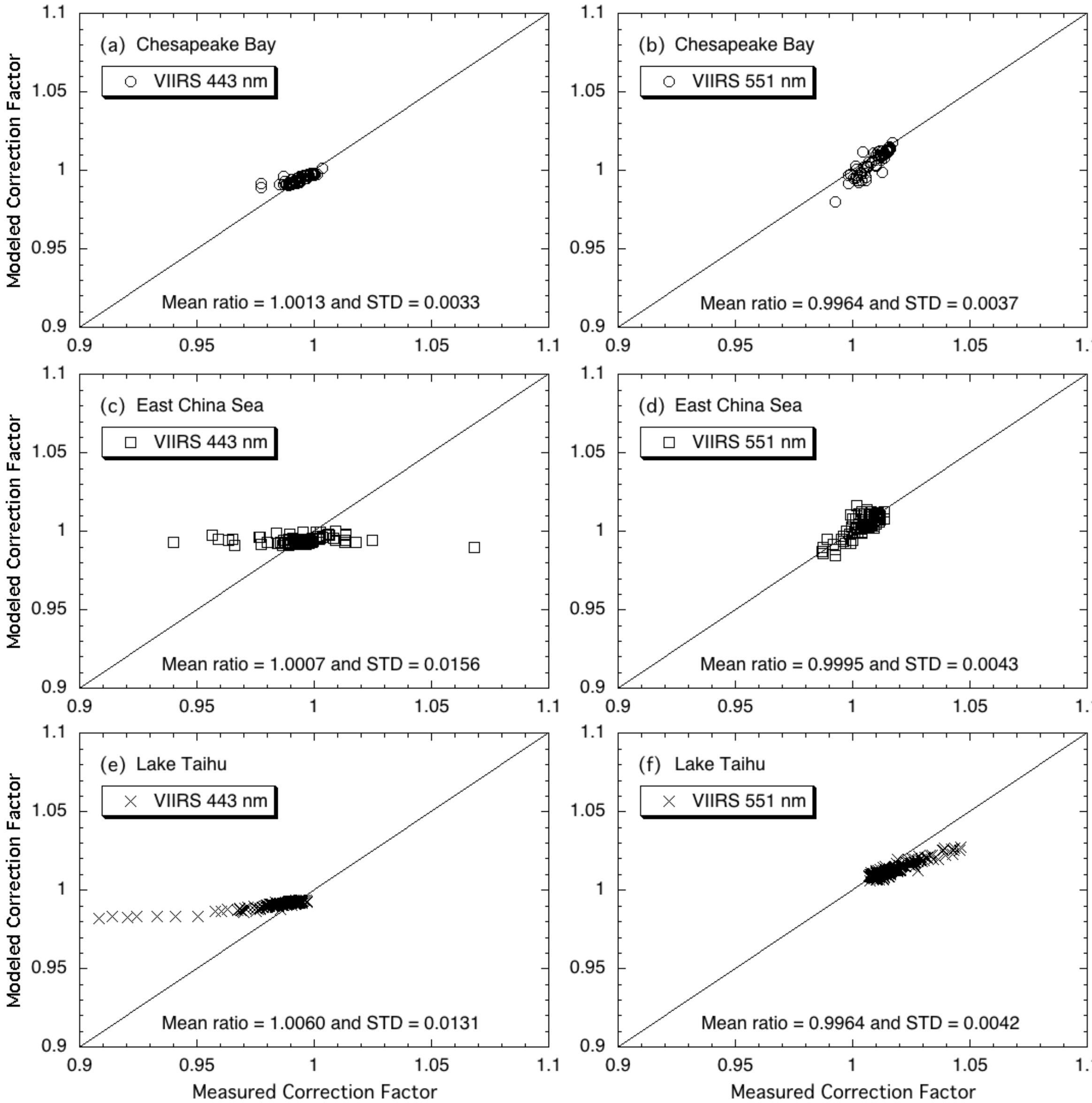

Figure 4. VIIRS results of the OOB correction factors derived from the correction formula Eq. (14) in comparison with those of true values for VIIRS bands of 443 and 551 nm with the water region of (a) and (b) Chesapeake Bay, (c) and (d) East China Sea, and (e) and (f) Lake Taihu.